Liu PP, Feng R, Wang FY, Xu Y, Zhu J-H. Fatigue testing of corroded RC continuous beams strengthened with polarized C-FRCM plate under ICCP-SS dual-function retrofitting system. Structures. 2022.

Fatigue testing of corroded RC continuous beams strengthened with polarized C-FRCM plate under ICCP-SS dual-function retrofitting system

Panpan Liu [a], Ran Feng [a*], Fangying Wang [b], Ying Xu [a], Ji-Hua Zhu [c]

[a] *School of Civil and Environmental Engineering, Harbin Institute of Technology, Shenzhen, China (518055)*

[b] *Department of Civil Engineering, University of Nottingham, United Kingdom*

[c] *Guangdong Provincial Key Laboratory of Durability for Marine Civil Engineering, College of Civil and Transportation Engineering, Shenzhen University, Shenzhen, China (518060)*

Abstract

The paper presents an experimental investigation into fatigue behaviour of corroded reinforced concrete (RC) continuous beams strengthened by carbon-fabric reinforced cementitious matrix (C-FRCM) under a typical dual-function retrofitting system. The retrofitting system adopted impressed current cathodic protection (ICCP) technique, which is an electro-chemical anti-corrosion technique for anodic polarization to reduce or prevent oxidation of metal, together with structural strengthening (SS) technique, which can effectively restore or improve the bearing capacity of the structure. In the experimental programme, a total of ten RC continuous beam specimens were tested under fatigue loading. The influence of key structural parameters on the fatigue life of the RC beams was examined, including the corrosion degree of the steel bar, fatigue load level, and charge density of C-FRCM plate. The calculation theory based on the transformed-section method for the cyclic stress amplitude of steel reinforcing bar in RC beam strengthened by C-FRCM plate was determined. On this basis, the *S*-*N* (cyclic stress amplitude versus cycles to failure) curves of the corroded RC continuous beams strengthened by polarized C-FRCM under the ICCP-SS dual-function retrofitting system were obtained by fitting the relevant

*Corresponding author, *E-mail address*: fengran@hit.edu.cn (R. Feng).

fatigue data for fatigue design guidance.

Keywords: Carbon-fabric reinforced cementitious matrix (C-FRCM); Continuous beam; Corroded; Fatigue test; ICCP-SS; Reinforced concrete (RC)

Notations

a_1	Ratio of the compressive strength of the prism to the compressive strength of the cube
A_f	Area of CF mesh of C-FRCM plate
A_s	Area of the tensile longitudinal rebar
A'_s	Area of the compressive longitudinal rebar
b	Normal cross-sectional width of RC beam
e	Charge density
E_c^f	Fatigue deformation modulus of concrete
E_l	Elastic modulus of uncorroded longitudinal rebar
E_{lc}	Elastic modulus of corroded longitudinal rebar
f_{cu}	Compressive strength of concrete cube
F_{max}	Upper limit of fatigue loading
F_{min}	Lower limit of fatigue loading
h_0	Distance from edge of the compression zone to centroid of the longitudinal rebar in the tension zone when the bending moments M_{max}^f and M_{min}^f are in the same direction
I_0^f	Moment inertia of transformed section for unstrengthened specimen when the bending moments M_{max}^f and M_{min}^f are in the same direction
I_{0f}^f	Moment inertia of transformed section for strengthened specimen when the bending moments M_{max}^f and M_{min}^f are in the same direction
M_{fe}	Mid-span bending moment at east side before fatigue failure of RC beam
M_{fm}	Bending moment of mid-support before fatigue failure of RC beam
M_{fw}	Mid-span bending moment at west side before fatigue failure of RC beam
M_{ie}	Mid-span bending moment under initial cyclic loading at east side
M_{im}	Bending moment of mid-support under initial cyclic loading

M_{iw}	Mid-span bending moment under initial cyclic loading at west side
M^{f}_{max}	Maximum bending moment at the same normal cross-section for fatigue calculation
M^{f}_{min}	Minimum bending moment at the same normal cross-section for fatigue calculation
S_{fit}	Fatigue stress amplitude given by calculation method
S_R	Fatigue stress amplitude given by the reference
x_0	Height of compression zone of the transformed section of the unstrengthened specimen
x_{0f}	Height of compression zone of the transformed section of the specimen strengthened with C-FRCM plate
α^{f}_{E}	Ratio of elastic modulus of the steel bar to the fatigue deformation modulus of concrete
α^{f}_{Ef}	Ratio of elastic modulus of the CF mesh to the fatigue deformation modulus of concrete
β_e	Mid-span bending moment redistribution of east side
β_m	Bending moment redistribution at mid-support
β_w	Mid-span bending moment redistribution of west side
ε_{cfu}	Ultimate tensile strain of CF mesh
ε_{lu}	Ultimate tensile strain of uncorroded longitudinal rebar
ε_{luc}	Ultimate tensile strain of corroded longitudinal rebar
ρ	Corrosion degree of longitudinal rebar
σ_{bcm}	Bending strength of cementitious matrix
σ_{cf}	Tensile strength of CF mesh
σ_{cm}	Compressive strength of cementitious matrix
σ_{lu}	Ultimate strength of uncorroded longitudinal rebar
$\sigma_{lu,c}$	Ultimate strength of corroded longitudinal rebar
σ_{ly}	Yield strength of uncorroded longitudinal rebar
σ_{lyc}	Yield strength of corroded longitudinal rebar
$\sigma^{f}_{s,max}$	Upper limit of fatigue stress given by the calculation method
$\sigma^{f}_{s,min}$	Lower limit of fatigue stress given by the calculation method

$\sigma_{s,max}^{R}$	Upper limit of fatigue stress given by the reference
$\sigma_{s,min}^{R}$	Lower limit of fatigue stress given by the reference
σ_{su}	Ultimate strength of uncorroded stirrup
σ_{sy}	Yield strength of uncorroded stirrup

1. Introduction

FRP strengthening technology has been widely utilised in the field of civil engineering for approximately two decades, owing primarily to the combined advantages of light weight, easy application, good strengthening effect, convenient construction, reduced building space, and limited negative influence on the aesthetic appearance of the structures. FRP is generally applied to the outer surface of reinforced concrete (RC) structures by using epoxy adhesive. However, the poor compatibility of epoxy resin with the concrete substrate usually leads to delamination of composite materials [1-2]. Moreover, epoxy resin exhibits a glassy transition in areas subjected to high temperature and fire hazards, which greatly impairs the adhesion between the carbon fiber and the concrete substrate. To resolve this, structural strengthening (SS) technique with fabric reinforced cementitious matrix (FRCM) system has been recently proposed [3]. Compared to traditional FRP strengthening, the FRCM strengthening provides superior mechanical and physical properties, including compatibility with concrete substrate, high temperature resistance, ultraviolet radiations, moisture resistance and fire resistance [4-7]. Thus, the FRCM strengthening has clear potential for applications in aggressive and demanding environments, such as places with extremely high temperature or prone to fire, and coastal or marine engineering sectors with high concentration of chloride ions, where the SS technique is deemed to be well suited.

The traditional SS technique can only improve the bearing capacity and unable to hinder the further development of the corrosion of RC structures. Anti-corrosion research of RC structures has become an important aspect of structural durability research. Impressed current cathodic protection (ICCP) technique has previously been recognized as an effective way to prevent steel corrosion in the chloride environment [8]. However, it can neither compensate for the reduction in bearing capacity owing to the loss of the effective cross-sectional area of the steel bar, nor can it recover the reduction in the bond strength between the corroded steel bar and concrete. It is undeniable that the two techniques have their advantages and disadvantages. With the trend to move to a low carbon economy, retrofitting and repairing deteriorated RC buildings, rather than demolition, is anticipated to be prioritised in the construction sector. Therefore, a combination technique of the relatively new SS technique and well-established ICCP technique, i.e. ICCP-SS dual-function retrofitting system is established for an improved repairing approach. During the operation of ICCP technique, the anode performance can be degraded, thus the selection of auxiliary anode is critical. The carbon-fabric (CF) mesh (as shown in Fig. 1a) offers excellent conductivity and mechanical properties [4] and therefore was adopted in the study as an auxiliary anode. The cementitious matrix has the advantages of good high-temperature resistance, compatibility with concrete, and good durability [5, 9], the FRCM plate made of the above two materials is suitable as the anode material and strengthening material of the ICCP-SS dual-function retrofitting system.

Up to now, FRCM has been proven to be capable of strengthening RC structures with rather promising results [10-13]. To date, previous research has been primarily focused on the static behaviour of FRCM plate strengthened members. In particular, Ebead et al. [10] studied the static bending behaviour of RC beams strengthened with different layers of FRCM, and the results showed that RC beams strengthened with a single layer and double layers of C-FRCM exhibited premature fabric slippage from the mortar matrix, whereas beams strengthened with three layers of C-FRCM failed due to delamination of FRCM plates from the concrete substrate. Su et al. [11] investigated the structural responses, moment redistributions and evaluated the design rules of RC continuous beams with ICCP-SS system. Ascione et al. [12] proposed a procedure that combined the results of direct tensile and shear bond tests to provide design parameters for externally bonded FRCM plates. The research in Awani et al. [5] provided enlightenment for the bonding, flexural and shear properties of FRCM strengthened RC members. Babaeidarabad et al. [13] carried out analysis and design and provided well-established formulas to calculate the bearing capacities of the beams strengthened with two different FRCM strengthening schemes. Overall, there have been a considerable number of previous studies on the static behaviour of RC structures strengthened with FRCM.

Up to now, the design of fatigue behaviour of RC structures strengthened with FRCM has not been established. The maximum fatigue stress of different FRP is specified in the specifications ACI 549.4R-13 [14], AC 434-0616-R1 [15] and ACI 440.2R-08 [16], yet it is recommended that the steel stress range of CFRP strengthened beam should be limited to that of unstrengthened beam in the fatigue design of FIB Bulletin 14 [17]. In addition, there have been relatively few previous studies on fatigue behaviour of RC beams strengthened with FRCM. Gencoglu and Mobasher [18] studied the effect of the type and layer of fiber on the fatigue flexural behaviour of RC beams strengthened with alkali-resistant glass and polyethylene fabric impregnated with cement paste. The results showed that the fiber made an important contribution to the flexural capacity, and the increase in bending capacity altered the failure mode from bending failure to shear failure. Pino et al. [19] studied the fatigue behaviour parameters of RC beams strengthened with polyparaphenylene benzobisoxazole (PBO)-FRCM plate, particularly on their failure modes and fatigue residual strengths. Hadad et al. [20] tested 12 RC beams strengthened with FRCM plate and analysed the influence of the fiber architecture and strengthening ratio of FRCM; the results showed that the fatigue fracture of steel bar was the main reason for the failure and the FRCM can prolong the fatigue life by controlling crack growth in concrete. Overall, the current research into FRCM strengthened RC beam mainly focused on analyzing experimental data, the cyclic stress amplitude versus cycles to failure (*S*-*N*) curves were not given, and there was a lack of in-depth theoretical analysis. Furthermore, the research into the fatigue performance of strengthened members under the ICCP-SS dual-function retrofitting system is rarely explored. Feng et al. [21] tested the fatigue behaviour of four RC continuous beams with one type of fatigue load level, using ICCP-SS dual-function retrofitting system. However, one type of fatigue load level is not enough to establish the *S*-*N* behaviour under the ICCP-SS dual-function retrofitting system, especially considering that the C-FRCM plate is degraded and acidified after energization [4, 22]. Investigation into the influence of vital structural parameters on the fatigue life and fatigue life prediction of C-FRCM strengthened RC structures under the ICCP-SS dual-function retrofitting system has become imperative, and this is the focus of the current study.

In this paper, fatigue testing of ten RC continuous beams, considering two types of fatigue load levels, is presented. The experimental results are first discussed, including fatigue life, failure modes, cracks in concrete, mid-span deflection, tensile strain of steel reinforcing bars and moment redistribution of internal force. Then, the effects of fatigue load level, charge density of C-FRCM plate, corrosion degree of steel bar on the fatigue behaviour of specimens are analyzed. The calculation theory for the cyclic stress amplitude of steel reinforcing bar is obtained on the basis of the transformed-section method in RC beam strengthened with C-FRCM plate. Finally, based on the stress amplitude theory of steel bar, the *S*-*N* curves of the corroded RC continuous beams strengthened with polarized C-FRCM plate are obtained by fitting the relevant fatigue data for fatigue design guidance.

2. Experimental investigation

2.1. Details of specimens

An experimental programme was carried out to investigate the fatigue behaviour of RC beams strengthened by C-FRCM. A total of ten RC continuous beam specimens was prepared with nominal cross-section dimensions of 150×250 mm. The nominal total length of the continuous beam was set as 2400 mm, and the effective length of a single span was 1100 mm. The specific dimensions and reinforcement are shown in Fig. 1a. The longitudinal reinforcement employed steel reinforcing bars with a diameter of 14 mm, and the stirrup adopts the steel reinforcing bar with a diameter of 8 mm spaced at 80 mm interval along the beam. The cross-sectional dimensions of RC beams strengthened with FRCM plates were identical to those of unstrengthened counterparts, with the only difference being the inclusion of C-FRCM plates with the size of 900×150 mm. The C-FRCM plates were located at the regions with relatively large bending moments and pasted on the top and bottom of RC continuous beams at mid-span, as shown in Fig. 1b.

In order to investigate the fatigue behaviour of the RC continuous beams strengthened with C-FRCM plate under ICCP-SS dual-function retrofitting system, ten specimens were divided into three categories, including unstrengthened uncorroded beams, unstrengthened corroded beams, and strengthened corroded beams, as listed in Table 1. The specimen labeling system (e.g. CB-P1-L2-0.40) starts with the letter 'CB' symbolising a corroded beam ('B' indicating an uncorroded beam), followed by 'L' with a number representing the layer of C-FRCM and 'P' with a number representing the degree of polarization, and ends with '0.40' or '0.25' designating the fatigue load level. It is worth noting that 'P0' represents no polarization, 'P1' represents the polarization effect achieved at a current density of 100 mA/m^2 and charge time of three months (charge density is the product of the current density and the charge time, which is 7.78×10^5 A·s/m^2 herein), 'P2' represents the polarization effect achieved at a current density of 150 mA/m^2 and charge time of 2.5 months (charge density is 9.72×10^5 A·s/m^2 herein).

2.2. Polarization of C-FRCM plate

The quality of prefabricated C-FRCM plate is one of the key points that need to be considered when implementing the ICCP-SS dual-function retrofitting system. A detailed description of the preparation process and the polarization device of the C-FRCM plate were given in Ref. [21]. Generally, the ICCP-SS dual-function retrofitting system should be carried out on the specimen, that is, the in-situ test, the steel bar is functioning as the cathode, and the CF mesh in the C-FRCM plate is acting as the anode, so as to achieve the dual function of preventing the steel bar from corrosion and enhancing the bearing capacity of the specimen. Considering that the effectiveness of the ICCP technology has been confirmed [22-24], the impact of electrode polarization of the C-FRCM plate is the focus of the study. Moreover, in order to reduce the test time and cost consumption, the prefabricated polarized C-FRCM plate was employed for the experimental programme. The curing process in the study is as follows: (a) Affix the surface of newly fabricated C-FRCM plate with plastic wrap to keep the C-FRCM plate with enough moisture; (b) Then put it in a moist environment for hardening; (c) Take off the plastic wrap and remove the mould after hardening; (d) Place the C-FRCM plate in a standard curing room for 28 days. Specifically, the C-FRCM plate after curing was electrically polarized in the laboratory environment to reach the corresponding degree of polarization and charge time, prior to be pasted on the RC beam, as shown in Fig. 2. This is to ensure that the deterioration and strength degradation of the C-FRCM under the current situation were consistent with the in-situ test results.

2.3. Material properties

Material testing was conducted to obtain the compressive strengths of concrete and cementitious matrix, as well as tensile strengths of steel bar and CF mesh. The measured material properties are summarised in Table 2 with typical material testing photographs shown in Fig. 3. The details of the tensile strength and flexural strength of C-FRCM plate can be found in Ref. [21].

2.4. Test loading scheme

Prior to fatigue tests, the control beam was statically loaded to determine the fatigue load level. The control beam employed in this study is consistent with that of Ref. [21]; the bearing capacity at the yielding of steel bar is 320 kN and ultimate bearing capacity is 436 kN. The upper limits of the fatigue loads were set as 0.40 and 0.25 times of the ultimate load, thus the fatigue load levels were 0.40 and 0.25 with 0.2 of the stress ratio, respectively. The fatigue loading scheme adopted 5 Hz as the loading frequency, the sine wave as the loading waveform, and the load-controlled loading system. MTS quasi-dynamic testing machine with the maximum loading capacity of 1000 kN was utilised for the fatigue testing of RC continuous beams with a five-point bending configuration, as shown in Fig. 4. The fatigue steps were carried out in accordance with the code [25], and the entire loading process was divided into three stages: preloading stage, static loading stage and fatigue loading stage, as shown in Fig. 4a. In the preloading stage, the loading rate of 0.3 kN/s was used up to 10 kN and stable for several minutes to ensure that the loading device and acquisition equipment worked normally. In the static loading stage, the loading rate of 0.3 kN/s was carried out for three static loading/unloading cycles and the maximum load was the upper limit of the fatigue cycle (F_{max}). In the fatigue loading stage, once the fatigue load cycles reached 1000, 5000, 10,000, 30,000, 50,000, 100,000, 200,000, 300,000, 500,000, 700,000, 1 million, 1.5 million, and 2 million times, one final static loading/unloading cycle should be carried out with the loading rate of 0.3 kN/s. It is worth noting that in the case that the specimen did not fail after the fatigue cycle reaches 2 million times, static loading was performed until the failure of the specimen.

2.5. Layout of measuring points

The instrumentation employed for fatigue testing of the RC continuous beam is shown in Fig. 4b, where linear variable displacement transducers (LVDTs) were installed at the end supports and middle of each span to measure the displacement, strain gauges were sticked onto reinforcing bars to measure the strain development, and the load cells were positioned at loading actuator and end supports to obtain the loading in the continuous beam. The locations of strain gauges on the steel bars are shown in Fig. 5, where identification system (e.g. W1) starts with the letter 'W' symbolizing west side ('E' indicating east side, and 'M' indicating mid-support), and ends with number '1' symbolizing front side of beam ('2' indicating back side).

2.6. DIC application

Digital image correlation (DIC) technology has been proven to be an economic, effective, user-friendly and accurate method for examining crack initiation and propagation. By processing the speckle image, the cloud images of the displacement field and strain field on the surface of the specimen are obtained. The basic principle is to use the gray scale of the speckle image as the carrier of specimen deformation information to track the speckles on the series of pictures for the matched specimen, so as to calculate the displacement information of the specimen in the deformation process. The principle is visualised in Fig. 6, where the displacement information of the center point can be obtained by analyzing the displacement vector of the center point of multiple continuous deformation sub-zones. DIC technology was utilised to calculate the development of concrete cracks in this study. The device arrangement is shown in Fig. 7, where industrial camera, data collector, computer and lighting source were included to ensure accurate measurements, and VIC-2D software was used for correlation after image acquisition.

3. Analysis of test results

3.1. Corrosion degree of steel bar

The longitudinal reinforcing bars embedded in the specimens were chiseled for pickling after the test. The corrosion degree of the steel bars was measured by the weight reduction of steel bars before and after rust removal. The measured weight reduction, taken as the weight loss of the total weight before rust removal, are presented in Table 1. It was apparent that generally significant weight reduction values were observed for corroded beams, indicating the existence of severer corrosion compared to uncorroded beam specimens. A comparison of steel bars before and after rust removal is presented in Fig. 8.

3.2. Failure modes

3.2.1. Failure modes of specimens at a fatigue load level of 0.40

The failure modes and crack development of a total of five RC continuous beams at a load level of 0.40 are shown in Fig. 9. For the unstrengthened specimens B-L0-P0-0.40 and CB-L0-P0-0.40, failures occurred when the longitudinal rebars yielded along with the crushing of concrete. For the strengthened specimen CB-L2-P0-0.40, the C-FRCM plates at the mid-span of two spans cracked earlier than the C-FRCM plate at the mid-support followed by the crushing of concrete, and the fracture of longitudinal rebar was finally regarded as the end of the test. This phenomenon also appeared on the specimens CB-L2-P1-0.40 and CB-L2-P2-0.40. The failure modes for the above-mentioned test specimens are summarised in Table 3.

The fatigue life for each test specimen was measured and presented in Table 3. For those with fatigue life over 2 million cyclic loading, the residual bearing capacities were presented for comparison purpose. For a group of unstrengthened specimens with a fatigue load level of 0.40, the fatigue life of the unstrengthened uncorroded specimen B-L0-P0-0.40 is 52.2×10^4 times, whereas the fatigue life of the unstrengthened corroded specimen CB-L0-P0-0.40 is 32.5×10^4 times. The significant longer fatigue life for uncorroded specimen with respect to the corroded reference specimen, indicates that the detrimental effect of corrosion in steel bars on fatigue performance of RC beams is significant. The decrease in strength caused by the corroded steel bars has a negative impact on the fatigue life of the specimen. For the specimens CB-L2-P0-0.40 and CB-L2-P2-0.40, between which the corrosion degree of the steel bars was close, fatigue life of the former specimen with untreated C-FRCM plate is 90.1×10^4 times, while the fatigue life of the latter specimen strengthened with polarized C-FRCM plate is 38.8×10^4 times. This difference reveals that the polarization of the C-FRCM plate caused by the energization lead to the decrease in the strength of the C-FRCM plate, thereby a reduced strengthening effect.

3.2.2. Failure modes of specimens at a load level of 0.25

Fatigue failures did not occur on the group of specimens with a fatigue load level of 0.25, after 2 million fatigue cycles. According to the requirements given in GB/T 50152-2012 [25], static loading is utilised until the failure of specimens for the undamaged specimens after 2 million fatigue cycles. The displacement loading was applied with a loading rate of 0.2 mm/min. The failure modes of these specimens obtained by static loading following fatigue loading are displayed in Fig. 10. It can be seen that the ductilities of specimens CB-L2-P1-0.25 and CB-L2-P2-0.25 strengthened with polarized C-FRCM plate are worse with negligible crack development than that of the specimen CB-L2-P0-0.25 strengthened with untreated C-FRCM plate, indicating that the specimens with polarized C-FRCM plate were brittle and more prone to sudden failure. Overall, it is concluded that the deterioration of C-FRCM plates reduces the bearing capacities of the specimens (as shown in Table 3), and reduces the ductility of the specimens. The strength reduction and ductility deterioration resulted from the corrosion of steel bars also increases the brittleness of the specimens.

3.3. Development of concrete cracks

Concrete crack strains of the specimen B-L0-P0-0.40 observed with DIC technology after a certain cycle of fatigue loading are shown in Fig. 11. It can be seen that the main cracks generally formed at the initial 1,000 times of cyclic loading. With the increase of cycles, the main cracks continued to develop and widened followed by the appearance of secondary cracks. It was also observed that the cracks at the mid-span of the east side are more obvious than those of the west side. As a consequence, the final damage occurred at the mid-span of the east side.

3.4. Development of mid-span deflections

The fatigue behaviour of all the test specimens is examined through mid-span deflection-cycle times curves, as presented in Fig. 12. The curves are deemed to be a comprehensive indication of fatigue performance, with regards to the process of concrete cracking, crack development and the change of the bond-slip behaviour of the steel bar and concrete during the fatigue test. For the group of specimens with a fatigue load level of 0.40, the deflection development can be categorised into almost three-stage: the deflection of the specimens develops rapidly before the cycle reaching 1000 times; the deflection of the specimens gradually stabilizes with the increases of cycles; then the deflection develops rapidly until the failure of specimens. For the group of specimens with a load level of 0.25, the deflection development is relatively stable at the initial stage of fatigue load, and the deflection almost remained unchanged in the later stage of fatigue load.

3.5. Development of strains of longitudinal rebars

The general trends of strain development of longitudinal rebars, as presented in Figs. 13 and 14, are essentially similar to those of mid-span deflection with the increase of cycle times. The development of strain is mainly attributed from the accumulation of residual strain of longitudinal rebars, which reflects the gradual deterioration of the mechanical properties of longitudinal rebars under cyclic loading. This is a process of accumulation of fatigue damage. Therefore, in the fatigue design of corroded flexural specimen, the strain of longitudinal rebars under cyclic loading is one of the main factors that need to be considered.

The strain development of longitudinal rebars in the group of specimens with a load level of 0.40 is shown in Fig. 13. It can be seen that the strains of the longitudinal rebars also increase rapidly in the early stage, which may be attributed to the fast development of concrete deterioration in the early stage of fatigue loading and the strains of rebars developed with the move of the neutral axis within the cross-section. During relatively stable stage, the strain of steel bars developed steadily when concrete cracks development slowed down. Compared with unstrengthened specimens, the strains of longitudinal rebars of the strengthened specimens CB-L2-P0-0.40 and CB-L2-P1-0.40 are smaller than those of the unstrengthened specimens B-L0-P0-0.40 and CB-L0-P0-0.40. This indicates that the CF mesh contributed to tensile force within the cross-sections and reduce the stress in the longitudinal rebars. However, for the specimen CB-L2-P2-0.40 with a large degree of polarization of the C-FRCM plate, the tensile force borne by the deteriorated CF mesh was reduced.

The strain development of longitudinal rebars in the group of specimens with a load level of 0.25 is shown in Fig. 14. It can be seen that due to the small amplitude of the cyclic loading, the plastic strain of longitudinal rebars was not obvious at the elastic stage, and the residual strain accumulation was insignificant. From the initial stage to the later stage of fatigue loading, the concrete cracks developed extremely slowly and the neutral axis remained unchanged, the strains of the longitudinal rebars also appeared relatively stable. Compared with the unstrengthened specimens, the strain development of longitudinal rebars of strengthened specimens B-L2-P0-0.25, CB-L2-P1-0.25 and CB-L2-P2-0.25 were lower than those of the unstrengthened specimens B-L0-P0-0.25 and CB-L0-P0-0.25. In addition, it should be noted that due to the long-term artificial corrosion of specimens, the corrosion degree of individual specimen is relatively large, especially for CB-L2-P2-0.25, which causes the damage of strain gauges on steel bars.

3.6. Moment redistribution

In the process of fatigue loading, due to the continuous development of cracks, the stiffness of the specimen changes constantly. The force of each cross-section is different, and the material damage degree is also different. Therefore, in the process of the whole fatigue loading, the RC continuous beam shows a redistribution phenomenon of internal force. The effect of bending moment redistribution under fatigue cyclic loading was examined herein. The bending moment value at the initial cyclic loading is defined as M_i, the bending moment value at the end of the cyclic loading is defined as M_f, and the bending moment redistribution formula under fatigue loading is defined as:

$$\beta = \frac{M_i - M_f}{M_i} \times 100\% \tag{1}$$

The moment redistribution of test specimens is shown in Table 4. It is observed that the differences between the moment redistribution values of mid-span of the west side and that of mid-span of the east side were apparent for a group of specimens with a load level of 0.40. For a group of specimens with a load level of 0.25, after 2 million cycles, the specimens did not show obvious failure characteristics. Hence, the difference in the moment redistribution between the mid-span of the east side and the mid-span of the west side for each specimen was not significant. In general, the cross-section internal force of RC continuous beam was constantly changing during the process of fatigue loading, and moment redistribution occurred on all specimens, especially for the mid-span of failure side.

4. Stress amplitude of steel bar

The fatigue behaviour of the specimen is measured by the fatigue strength (i.e. the strength of the specimen under alternating loads) and the fatigue strength is measured by the fatigue limitation (i.e. the maximum stress that specimen can withstand infinite cycles without fatigue failure under a certain stress ratio). The fatigue curve or *S*-*N* curve is demonstrated as the relationship between the stress amplitude of steel bar and fatigue life or the cycle. Fatigue failure is generally exhibited as the sudden fatigue fracture of longitudinal rebar, which leads to the fatigue failure of the entire specimen. Therefore, the fatigue strength of the specimen mainly depends on the fatigue strength of the longitudinal rebar. However, in the existing studies [21], the fatigue load was not converted into the fatigue stress of the longitudinal rebar and the *S*-*N* curve was not given. In order to more accurately describe and investigate the fatigue behaviour of the C-FRCM strengthened specimens under the ICCP-SS dual-function retrofitting system, the calculation theory of the fatigue stress amplitude of unstrengthened and strengthened specimens with polarized C-FRCM plate was proposed.

Before the fatigue failure of the RC beam, the internal stress of the member is small, and is basically still in the elastic stage. Therefore, the proposed method for the fatigue calculation was based on homogeneous elastic material. The main principle is to obtain the equivalent homogeneous material conversion section through the conversion of the ratios of elastic modulus of longitudinal rebar and CF mesh. The corresponding calculation formulas were derived and established according to the elastic mechanical method.

4.1. Stress amplitude of steel bar for unstrengthened RC beams

In order to obtain the fatigue stress of the cross-section of the flexural member, the following assumptions need to be adopted [26]:

- Sectional strain maintains plane;
- The normal stress pattern of the concrete at the compression zone is taken as a triangle; Regardless of the tensile strength of the concrete at the tension zone, the tensile force of the RC member is borne by the longitudinal rebar;
- Calculation using transformed-section method.

A simplified diagram of the fatigue stress of the nominal cross-section of the unstrengthened flexural member is displayed in Fig. 15. The general formulas of stress amplitude of longitudinal rebars for unstrengthened RC flexural members are given in Eqs. 2-4, according to Chinese code for RC structures [26].

$$S = \Delta\sigma_{s,max}^{f} - \Delta\sigma_{s,min}^{f} \tag{2}$$

$$\sigma_{s,min}^{f} = \alpha_{E}^{f} \frac{M_{min}^{f}\left(h_0 - x_0\right)}{I_0^{f}} \tag{3}$$

$$\sigma_{s,max}^{f} = \alpha_{E}^{f} \frac{M_{max}^{f}\left(h_0 - x_0\right)}{I_0^{f}} \tag{4}$$

where M_{max}^{f} and M_{min}^{f} are the maximum and minimum bending moment capacities, respectively, at the same nominal cross-section during fatigue stress calculation; $\sigma_{s,max}^{f}$ and $\sigma_{s,min}^{f}$ are the stresses of the longitudinal rebars in the tensile zone of the corresponding section resulted from the bending moments M_{max}^{f} and M_{min}^{f}, respectively; α_{E}^{f} is the ratio of elastic modulus of the longitudinal rebars to the fatigue deformation modulus of concrete, and the fatigue deformation modulus of concrete is shown in Table 5; I_0^{f} is the moment inertia of transformed section; x_0 is the compression zone height of the transformed section and h_0 is the distance from the edge of the compression zone to the centroid of the longitudinal rebars in the tension zone. Note that I_0^{f}, x_0 and h_0 were calculated on the basis of section where on the bending moments M_{max}^{f} and M_{min}^{f} are in the same direction during the fatigue calculation. The height of compression zone x_0 and the moment inertia I_0^{f} of the transformed section should be calculated according to the following formulas:

$$\frac{bx_0^2}{2}+\alpha_E^f A_s^{'}\left(x_0-a_s^{'}\right)-\alpha_E^f A_s\left(h_0-x_0\right)=0 \tag{5}$$

$$I_0^f=\frac{bx_0^3}{3}+\alpha_E^f A_s^{'}\left(x_0-a_s^{'}\right)^2+\alpha_E^f A_s\left(h_0-x_0\right)^2 \tag{6}$$

where b is the normal cross-sectional width of RC beam, A'_s is the cross-sectional area of the compressive longitudinal rebars and A_s is the cross-sectional area of the tensile longitudinal rebars.

The comparisons of the stress amplitudes of steel bars presented in Refs. [22, 27-29] and proposed theoretical method are presented in Table 6. It is evident that the stress amplitudes of longitudinal rebars obtained from references (S_R) are in good agreement with the theoretical calculation results (S_{fit}), with the mean value (S_R/S_{fit}) of 0.99 and the coefficient of variation (COV) of 0.101. It can be concluded that the proposed formulas are capable of predicting fatigue behaviour of unstrengthened specimens and can be used to calculate the stress amplitude of longitudinal rebars.

4.2. Stress amplitude of steel bar for strengthened RC beams

In order to predict the cross-sectional fatigue life of the C-FRCM strengthened members, in addition to the assumptions aforementioned in Section 4.1, an additional assumption should be made, i.e., no peeling failure occurs between the C-FRCM plate and concrete. A simplified diagram of the fatigue stress of the normal cross-section of the strengthened flexural member is shown in Fig. 15b. The calculation formulas for the compression zone height x_{0f} and the moment of inertia I_{0f}^f of the transformed section of the C-FRCM strengthened specimens are given in Eqs. 7-8.

$$\frac{bx_{0f}^2}{2}+\alpha_E^f A_s^{'}\left(x_{0f}-\alpha_s^{'}\right)-\alpha_E^f A_s\left(h_0-x_{0f}\right)-\alpha_{Ef}^f A_f\left(h-x_0\right)=0 \tag{7}$$

$$I_{0f}^f=\frac{bx_{0f}^3}{3}+\alpha_E^f A_s^{'}\left(x_{0f}-\alpha_s^{'}\right)^2+\alpha_E^f A_s\left(h_0-x_{0f}\right)^2+\left[\alpha_{Ef}^f A_f\left(h-x_{0f}\right)^2\right] \tag{8}$$

where α_{Ef}^f is the ratio of elastic modulus of the CF mesh in C-FRCM plate to the fatigue deformation modulus of concrete; A_f is the cross-sectional area of CF mesh of C-FRCM plate; x_{0f} is the height of compression zone of the transformed section of the C-FRCM strengthened specimen and I_{0f}^f is the moment inertia of transformed section of the C-FRCM strengthened specimens.

With reference to the calculation process of the stress amplitude of the longitudinal rebars of the unstrengthened specimens (see Eqs. 2-4), and combined with Eqs. 7-8, the stress amplitude of the longitudinal rebars of the strengthened specimens can be determined. Table 7 shows the comparison of stress amplitude given by Refs. [22] and [30] and calculated by the proposed method. It is obvious that S_R is relatively consistent with S_{fit}, with the mean ratio (S_R/S_{fit}) of 0.95 and the COV of 0.088. It can be seen that the proposed fatigue theory can be used to calculate the fatigue stress amplitude of longitudinal rebars of the strengthened specimens.

4.3. S-N curves

4.3.1. S-N curves for unstrengthened corroded specimens

The stresses of longitudinal rebars of specimens at fatigue load levels of 0.55, 0.40 and 0.25 are summarised in Table 7, where the test results at a fatigue load level of 0.55 are obtained from Ref. [21]. It is worth noting that corrosion can degrade the elastic modulus of the steel bar, therefore the elastic modulus for uncorroded steel bar presented in Table 2 cannot be used. To rectify this, the elastic modulus of uncorroded steel bar was converted into the elastic modulus of corroded steel bar, according to the following formulas proposed by Wu and Yuan [31]:

When $0 < \rho\% \leq 5\%$,

$$\begin{aligned} \sigma_{lyc} &= \sigma_{ly}\left(1-0.029\rho\right) \\ \sigma_{luc} &= \sigma_{lu}\left(1-0.026\rho\right) \\ \varepsilon_{luc} &= \varepsilon_{lu}\left(1-0.0575\rho\right) \\ E_{lc} &= E_{l}\left(1-0.052\rho\right) \end{aligned} \tag{9}$$

When $\rho\% > 5\%$,

$$\begin{aligned} \sigma_{lyc} &= \sigma_{ly}\left(1.175-0.064\rho\right) \\ \sigma_{luc} &= \sigma_{lu}\left(1.18-0.062\rho\right) \\ \varepsilon_{luc} &= \varepsilon_{lu}\left(1-0.0575\rho\right) \\ E_{lc} &= E_{l}\left(0.895-0.031\rho\right) \end{aligned} \tag{10}$$

where $\rho\%$ is the degree of corrosion of steel bar; E_l, σ_{ly}, σ_{lu} and ε_{lu} are the elastic modulus, yield strength, ultimate strength and ultimate strain of uncorroded steel bar, respectively; and E_{lc}, σ_{lyc}, σ_{luc} and ε_{luc} are the elastic modulus, yield strength, ultimate strength and ultimate strain of corroded steel bar, respectively.

The fatigue life N (i.e. cycle) is commonly determined by S-N method. The power function is used to describe the *S-N* curve [32-34], as given by Eq. 11.

$$S^m N = t \tag{11}$$

Taking the logarithm on both sides of Eq. 11, Eq. 12 was derived,

$$m\log S+\log N=\log t \tag{12}$$

where S is the stress amplitude, N is the fatigue life, and m and t are the parameters corresponding to stress ratio, rebar diameter, grade, and minimum cyclic loading.

It can be seen from Eq. 12 that when a power function is used, log$S$ and log$N$ are linear relation. Accounting for the influence of corrosion degree of steel bar, the above relationship can be transformed to:

$$A\log S+B\log N+C\log\rho\%=\log D \tag{13}$$

where A, B, C and D are the parameters related to materials. The values are obtained by conducting regression on the test data.

The data used herein includes stress amplitudes, fatigue life, and corrosion degree of longitudinal rebars of unstrengthened specimens, as presented in Table 7. Multiple linear regression analyses were conducted and the *S-N* curve of unstrengthened corroded specimens is given as follows:

$$\log N_{fit}=-0.055\log\rho\%-3.541\log S_{fit}+9.717 \tag{14}$$

where A is equal to 3.541, B is equal to 1.000, C is equal to 0.0055, and D is equal to $10^{9.717}$. Moreover, N_{fit} is the fitting fatigue life and S_{fit} is the fitting stress amplitude.

The comparison of the fatigue life of the unstrengthened corroded specimens is shown in Table 8. The logarithm of the test fatigue life (log$N$) is compared with the logarithm of the fitted fatigue life (logN_{fit}), with the mean value (log$N$/logN_{fit}) of 1.00, the COV of 0.039 as well as the coefficient of determination of 0.925. This reveals that the proposed equations yield a high level of accuracy and consistency for fatigue life predictions of the unstrengthened corroded specimens.

4.3.2. S-N curves for strengthened corroded specimens with polarized C-FRCM plate

With reference to the establish of the relationship between the stress amplitude, the corrosion degree of steel bar, as well as the fatigue life of the strengthened corroded specimens with polarized C-FRCM plate, and the introduction of the charge density (e), the *S-N* curves of the corroded RC beams strengthened with the polarized C-FRCM plate can be established as:

$$A\log S+B\log N+C\log\rho\%+G\log e=\log D \tag{15}$$

where A, B, C, D and G are the parameters related to materials. Again, these values were obtained by regression.

The stress amplitudes, corrosion degree of steel bars, and fatigue life of the specimens strengthened with polarized C-FRCM plate in Table 7 are taken the logarithm and subjected to multiple linear regression analyses. The S-N curve of the corroded RC beams strengthened with polarized C-FRCM plate is as follows:

$$\log N_{fit}=0.381\log\rho\%-2.857\log S_{fit}-1.918\log e+24.181 \tag{16}$$

where A is equal to 2.857, B is equal to 1.000, C is equal to -0.381, D is equal to $10^{24.181}$ and G is equal to 1.918. Moreover, N_{fit} is the fitting fatigue life and S_{fit} is the fitting stress amplitude.

The comparison of the fatigue life of the corroded specimens strengthened with the polarized C-FRCM plate is shown in Table 9. It is evidently shown that the mean value of $\log N/\log N_{fit}$ is 1.00, and the COV is 0.008, indicating that the accuracy of the proposed fatigue life prediction of corroded RC beams strengthened with polarized C-FRCM plate.

5. Conclusions

In the present study, the fatigue tests of ten RC continuous beams were carried out and fatigue behaviour of the specimens strengthened with C-FRCM plate under ICCP-SS dual-function retrofitting system was investigated. The influences of the corrosion degree of steel bar, the fatigue load level, and the charge density of the C-FRCM plate on the fatigue behaviour of RC continuous beams were discussed. In order to observe the development of cracks during fatigue loading, DIC technology was utilised; the failure modes and fatigue life of RC continuous beams under different load levels, the mid-span deflections, as well as strains of steel bars under certain cyclic loading were analysed. The following conclusions can be drawn:

- The C-FRCM plate was degraded due to polarization, resulting in a decrease of its strength, thus the strengthening effect was greatly reduced. Electrical polarization of C-FRCM plate and corrosion degree of steel bars were found to significantly affect the fatigue life of the specimens.
- In the process of fatigue loading of RC specimens, the main cracks of concrete were mostly concentrated in the early stage of fatigue loading, and the main cracks continued to expand and

fine cracks gradually occurred in the later stage of fatigue loading.

- The deflection law of mid-span of RC continuous beam was similar to the strain law of longitudinal rebar. The development of mid-span deflection differed significantly between load levels of 0.4 and 0.25. More rapid development and greater deflections were observed for specimens with higher load level.
- The *S*-*N* curves of unstrengthened corroded specimens and strengthened corroded specimens strengthened with polarized C-FRCM plates were derived based on stress amplitude calculation theory of steel bar; and have shown great accuracy for fatigue life predictions.

Acknowledgements

The authors are grateful for the financial support from Key-Area Research and Development Program of Guangdong Province (Grant No. 2019B111107002), National Key Research and Development Program of China (Grant No. 2018YFE0124900), National Natural Science Foundation of China (Grant Nos. 52178131/51538007/51778370/51861165204/51778191/52078173), Natural Science Foundation of Guangdong Province (Grant Nos. 2018A030313208/2017B030311004), Shenzhen Science and Technology Program (Grant No. GXWD20201230155427003-20200804174353001), Shenzhen Key Laboratory Launching Project (Grant No. ZDSYS20200810113601005).

References

[1] El-Maaddawy T, El-Ariss B. Behavior of concrete beams with short shear span and web opening strengthened in shear with CFRP composites. Journal of Composites for Construction, ASCE 2012, 16(1): 47-59.

[2] El-Maaddawy T, Chekfeh Y. Retrofitting of severely shear-damaged concrete T-beams using externally bonded composites and mechanical end anchorage, Journal of Composites for Construction, ASCE 2012, 16(6): 693-704.

[3] D'Ambrisi A, Focacci F. Flexural strengthening of RC beams with cement-based composites. Journal of Composites for Construction, ASCE 2011, 15(5): 707-720.

[4] Su MN, Wei LL, Zhu JH, Ueda T, Guo GP, Xing F. Combined impressed current cathodic protection and FRCM strengthening for corrosion-prone concrete structures. Journal of Composites for Construction, ASCE 2019, 23(4): 04019021.

[5] Awani O, El-Maaddawy T, Ismail N. Fabric-reinforced cementitious matrix: A promising strengthening technique for concrete structures. Construction and Building Materials, 2017, 132: 94-111.

[6] Nanni A. A new tool in the concrete and masonry repair-strengthening with fiber-reinforced cementitious matrix composites. Concrete International, 2012, 34(4): 43-49.

[7] Carozzi FG, Milani G, Poggi C. Mechanical properties and numerical modeling of fabric reinforced cementitious matrix (FRCM) systems for strengthening of masonry structures. Composite Structures, 2014, 107: 711-725.

[8] Weyers RE, Prowell BD, Sprinkel MM, Vorster M. Concrete bridge protection, repair, and rehabilitation relative to reinforcement corrosion: A methods application manual. Contract, 1993, 100: 103.

[9] Ombres L. Flexural analysis of reinforced concrete beams strengthened with a cement based high strength composite material. Composite Structures, 2012, 94(1): 143-155.

[10] Ebead U, Shrestha KC, Afzal MS, Refai EA, Nanni A. Effectiveness of fabric-reinforced cementitious matrix in strengthening reinforced concrete beams. Journal of Composites for Construction, ASCE 2017, 21(2): 04016084.

[11] Su MN, Zeng C, Li WQ, Zhu JH, Xing F. Flexural performance of corroded continuous RC beams rehabilitated by ICCP-SS. Composite Structures, 2019, 232: 111556.

[12] Ascione L, Felice GD, Santis SD. A qualification method for externally bonded fibre reinforced cementitious matrix (FRCM) strengthening systems. Composites Part B: Engineering, 2015, 78: 497-506.

[13] Babaeidarabad S, Loreto G, Nanni A. Flexural strengthening of RC beams with an externally bonded fabric-reinforced cementitious matrix. Journal of Composites for Construction, ASCE 2014, 18(5): 04014009.

[14] ACI 549.4R-13. Guide to Design and Construction of Externally Bonded Fabric-Reinforced Cementitious Matrix (FRCM) Systems for Repair and Strengthening Concrete and Masonry Structures. American Concrete Institute, Farmington Hills, USA, 2013.

[15] AC 434-0616-R1. Proposed Revisions to the Acceptance Criteria for Masonry and Concrete Strengthening using Fabric-Reinforced Cementitious Matrix (FRCM) Composite Systems. ICC Evaluation Service, Washington, DC, USA, 2016.

[16] ACI 440.2R-08. Guide for the Design and Construction of Externally Bonded FRP Systems for Strengthening Concrete Structures. American Concrete Institute, Farmington Hills, USA, 2008.

[17] FIB Bulletin 14. Externally Bonded FRP Reinforcement for RC Structures. International Federation for Structural Concrete, Zürich, Switzerland, 2001.

[18] Gencoglu M, Mobasher B. Monotonic and cyclic flexural behavior of plain concrete beams strengthened by fabric-cement based composites. Third International Conference on Structural Engineering, Mechanics and Computation (SEMC 2007). The Netherlands, Millpress, 2007, p. 1961-1966.

[19] Pino V, Hadad HA, Caso FD, Nanni A, Ebead UA, Refai AE. (2017). Performance of FRCM-strengthened RC beams subject to fatigue. Journal of Bridge Engineering, ASCE 2017, 22(10): 04017079.

[20] Hadad HA, Nanni A, Ebead UA, Refai AE. Static and fatigue performance of FRCM-strengthened concrete beams. Journal of Composites for Construction, ASCE 2018, 22(5): 04018033.

[21] Feng R, Wang J, Zhu JH, Dong ZJ. Fatigue behavior of corroded reinforced concrete continuous beams with multi-intervention system. Engineering Structures, 2021, 231: 111748.

[22] Wei LL. Characterizations of RC Beams Intervened by ICCP-SS System with Externally Bonded Carbon-FRCM Composites. PhD thesis, Hokkaido University, 2020.

[23] Zhu JH, Wei LL, Wang ZH, Ke LC, Fang Y, Xing F. Application of carbon-fiber-reinforced polymer anode in electrochemical chloride extraction of steel-reinforced concrete. Construction and Building Materials, 2016, 120: 275-283.
[24] Zhu JH, Wei LL, Moahmoud H, Redaelli E, Xing F, Bertolini L. Investigation on CFRP as dual-functional material in chloride-contaminated solutions. Construction and Building Materials, 2017, 151: 127-137.
[25] GB/T 50152-2012. Standard for Test Methods of Concrete Structures. China Building Industry Press, Beijing, China, 2012. (in Chinese)
[26] GB 50010. Code for Design of Concrete Structures. China Architecture & Building Press, Beijing, China, 2019. (in Chinese)
[27] Wan AZ. Experimental Study on Fatigue Behavior of the Damaged Reinforced Concrete Beam. PhD thesis, Central South University, Changsha, China, 2014. (in Chinese)
[28] Wu J, Wang CX, Xu J, Xiao Z, Wu FH. Study on flexural behavior of corroded reinforced concrete beams under fatigue loads. China Civil Engineering Journal, 2012, 45(10): 118-124. (in Chinese)
[29] Xing ML. Fatigue Test and Numerical Simulation of Corroded Reinforced Concrete Beam. PhD thesis, Shandong University, Jinan, China, 2013. (in Chinese)
[30] Dong YT, Ansari F, Karbhari VM. Fatigue performance of reinforced concrete beams with externally bonded CFRP reinforcement. Structure and Infrastructure Engineering, 2011, 7(3): 229-241.
[31] Wu Q, Yuan YS. Experimental study on the deterioration of mechanical properties of corroded reinforcing bars. China Civil Engineering Journal, 2008, 12(41): 42-47. (in Chinese)
[32] European International Concrete Committee, CEB/FIB Model Code 2010, London, UK, 2010.
[33] Barnes RA, Mays GC. Fatigue performance of concrete beams strengthened with CFRP plates. Journal of Composites for Construction, ASCE 1999, 3(2): 63-72.
[34] Zorn AV. Effect of Adhesive Stiffness and CFRP Geometry on the Behavior of Externally Bonded CFRP Retrofit Measures Subject to Fatigue Loads. PhD thesis, University of Pittsburgh, United States, 2006.

Specimen		Corrosion	Stress level	Layer of CF mesh	Charge density ($\times 10^5$ A·s/m^2)	Corrosion degree of rebar (%)
Unstrengthened uncorroded beam	B-L0-P0-0.40	N	0.40	0	0	0.83
	B-L0-P0-0.25	N	0.25	0	0	0.11
Unstrengthened corroded beam	CB-L0-P0-0.40	Y	0.40	0	0	3.86
	CB-L0-P0-0.25	Y	0.25	0	0	4.20
Strengthened corroded beam	CB-L2-P0-0.40	Y	0.40	2	0	6.01
	CB-L2-P1-0.40	Y	0.40	2	7.78	3.48
	CB-L2-P2-0.40	Y	0.40	2	9.72	6.52
	CB-L2-P0-0.25	Y	0.25	2	0	4.38
	CB-L2-P1-0.25	Y	0.25	2	7.78	3.78
	CB-L2-P2-0.25	Y	0.25	2	9.72	12.28

Table 1. Details of test specimens

Material		Strength (MPa)		E (GPa)
Concrete (C30)	Uncorroded	Compressive cubic strength f_{cu} (MPa)	27	—
	Corroded		26	
Rebar (Uncorroded)	ϕ8	Yield strength (σ_{ly})	356	197
		Ultimate strength (σ_{lu})	480	
	ϕ14	Yield strength (σ_{sy})	474	213
		Ultimate strength (σ_{su})	629	
CF mesh		Tensile strength (σ_{cf})	1333	118
		Ultimate tensile strain (ε_{cfu})	1.13%	
Cementitious matrix		Bending strength (σ_{bcm})	16	—
		Compressive strength (σ_{cm})	67	

Table 2. Material properties

Load level	Specimen	Fatigue life (×10^4 times)	Failure mode
0.40	B-L0-P0-0.40	52.2	A+B
	CB-L0-P0-0.40	32.5	A+B
	CB-L2-P0-0.40	89.1	A+B+C+D
	CB-L2-P1-0.40	42.2	A+B+C+D
	CB-L2-P2-0.40	38.8	A+B+C+D
Load level	**Specimen**	**Fatigue life (×10^4 times)**	**Residual bearing capacity (kN)**
0.25	B-L0-P0-0.25	>200	425.00
	CB-L0-P0-0.25	>200	388.60
	CB-L2-P0-0.25	>200	480.52
	CB-L2-P1-0.25	>200	473.54
	CB-L2-P2-0.25	>200	430.06

Note: A=Fracture of the longitudinal rebars at the mid-span, B=Local crush of concrete, C=Fracture of the C-FRCM plate at the mid-span, D=Fracture of the C-FRCM plate at the mid-support.

Table 3. Failure modes and residual bearing capacities of specimens

Load level	Specimen	Mid-span of west side			Mid-support			Mid-span of east side		
		M_{iw}	M_{fw}	β_w	M_{im}	M_{fm}	β_m	M_{ie}	M_{fe}	β_e
0.40	B-L0-P0-0.40	15.80	20.52	-30%	12.05	12.01	0.3%	18.18	18.19	-0.1%
	CB-L0-P0-0.40	12.55	15.34	-22%	12.20	10.75	11.9%	17.21	18.03	-4.8%
	CB-L2-P0-0.40	11.91	12.38	-4%	12.70	12.55	1.2%	17.85	17.93	-0.4%
	CB-L2-P1-0.40	12.33	17.59	-43%	10.56	10.35	1.9%	18.26	18.31	-0.3%
	CB-L2-P2-0.40	14.05	17.61	-25%	10.19	9.75	4.4%	17.82	18.28	-2.6%
0.25	B-L0-P0-0.25	10.97	11.20	-2.1%	6.73	5.54	17.8%	11.35	11.64	-2.5%
	CB-L0-P0-0.25	12.19	12.29	-0.9%	9.14	8.07	11.7%	9.92	10.42	-5.1%
	CB-L2-P0-0.25	10.19	10.74	-5.4%	8.69	7.64	12.1%	10.34	10.56	-2.1%
	CB-L2-P1-0.25	10.91	11.03	-1.1%	14.09	12.54	11.0%	8.34	9.13	-9.5%
	CB-L2-P2-0.25	9.83	9.28	5.6%	8.43	8.22	2.4%	10.00	10.38	-3.8%

Table 4. Moment redistribution of specimens

Strength grade	C30	C35	C40	C45	C50	C55	C60	C65	C70	C75	C80
E_c^f ($\times 10^4$ MPa)	1.30	1.40	1.50	1.55	1.60	1.65	1.70	1.75	1.80	1.85	1.90

Table 5. Fatigue deformation modulus of concrete

Reference	Specimen	Strengthening	$\sigma_{s,\max}^R$	$\sigma_{s,\min}^R$	S_R	$\sigma_{s,\max}^f$	$\sigma_{s,\min}^f$	S_{fit}	S_R/S_{fit}
Ref. [21]	C-B-L0-F55	N	271.20	98.30	172.90	309.27	112.56	196.71	0.88
	C-B-L0-F60		296.00	98.30	197.70	337.32	112.56	224.76	0.88
	C-B-L0-F70		345.70	98.30	247.40	393.43	112.56	280.86	0.88
Ref. [26]	—		221.00	47.00	174.00	228.82	45.76	183.05	0.95
Ref. [27]	L1		—	—	253.80	307.71	65.64	242.06	1.05
	L2		—	—	253.80	303.74	64.80	238.94	1.06
	L3		—	—	253.80	302.92	64.62	238.30	1.07
	L4		—	—	253.80	301.94	64.41	237.53	1.07
	L5		—	—	253.80	300.08	64.02	236.06	1.08
	L6		—	—	253.80	298.95	63.78	235.17	1.08
	L7		—	—	253.80	297.58	63.48	234.10	1.08
Ref. [28]	L-2		—	—	310.00	379.93	37.99	341.94	0.91
	L-3		—	—	315.00	383.35	38.34	345.05	0.91
	L-5		—	—	350.00	480.74	48.07	432.66	0.81
	L-8		—	—	366.00	374.25	37.43	336.83	1.09
Mean									0.99
COV									0.101
Ref. [21]	C-B-L1-F55	Y	244.40	83.40	160.90	292.27	106.37	185.90	0.87
	C-B-L1-F60		267.70	83.40	184.30	318.78	106.37	212.40	0.87
	C-B-L1-F70		314.90	83.40	231.50	371.79	106.37	265.42	0.87
	C-B-L2-F55		204.10	58.60	145.50	268.71	97.80	170.91	0.85
	C-B-L2-F60		226.50	58.60	167.90	293.08	97.80	195.28	0.86
	C-B-L2-F70		271.70	58.60	213.10	341.83	97.80	244.03	0.87
	C-B-L3-F55		187.00	43.00	144.00	248.66	90.50	158.16	0.91
	C-B-L3-F60		228.50	43.00	185.50	271.21	90.50	180.71	1.03
	C-B-L3-F70		270.90	43.00	228.00	316.32	90.50	225.82	1.01
Ref. [29]	F4-20A		—	—	279.70	332.91	66.58	266.33	1.05
	F4-26A		—	—	391.90	432.41	66.58	365.83	1.07
	F4-28		—	—	399.80	464.95	66.58	398.37	1.00
	F4-32		—	—	452.20	532.28	66.58	465.70	0.97
	F4-34		—	—	513.30	565.57	66.58	498.99	1.03
	F4-36B		—	—	561.20	598.87	66.58	532.28	1.05
Mean									0.95
COV									0.088

Table 6. Comparison of stress amplitudes given by references and theoretical method

Load level	Specimen	Corrosion degree of rebar (%)	P_{min} (kN)	P_{max} (kN)	$\sigma^f_{s,max}$ (MPa)	$\sigma^f_{s,min}$ (MPa)	S (MPa)	N ($\times 10^4$ times)
0.55	B-L0-P0-0.55	0.00	48.00	240.00	357.28	71.46	285.82	19.68
	CB-L0-P0-0.55	3.64	48.00	240.00	357.26	71.45	285.81	11.70
	CB-L2-P0-0.55	3.17	48.00	240.00	355.54	71.11	284.43	25.29
	CB-L2-P1-0.55	3.34	48.00	240.00	355.54	71.11	284.43	22.51
	CB-L2-P2-0.55	3.85	48.00	240.00	355.53	71.11	284.43	14.60
0.40	B-L0-P0-0.40	0.83	35.20	176.00	262.00	52.40	209.60	52.21
	CB-L0-P0-0.40	3.86	35.20	176.00	261.99	52.40	209.59	32.50
	CB-L2-P0-0.40	6.01	35.20	176.00	260.10	52.02	208.08	89.90
	CB-L2-P1-0.40	3.48	35.20	176.00	261.11	52.22	208.88	42.21
	CB-L2-P2-0.40	6.52	35.20	176.00	260.10	52.02	208.08	38.81
0.25	B-L0-P0-0.25	0.11	22.40	112.00	166.73	33.35	133.38	>200.00
	CB-L0-P0-0.25	4.20	22.40	112.00	166.72	33.34	133.38	>200.00
	CB-L2-P0-0.25	4.38	22.40	112.00	166.16	33.23	132.92	>200.00
	CB-L2-P1-0.25	3.78	22.40	112.00	166.16	33.23	132.93	>200.00
	CB-L2-P2-0.25	12.28	22.40	112.00	165.51	33.10	132.41	>200.00

Table 7. Stress amplitudes of longitudinal rebars of specimens at various load levels

Specimen	N ($\times 10^4$ times)	$\log N$	$\log N_{fit}$	$\log N/\log N_{fit}$
B-L0-P0-0.55	19.68	1.29	5.29	5.31
B-L0-P0-0.40	52.21	1.72	5.72	5.64
CB-L0-P0-0.55	11.70	1.07	5.07	5.05
CB-L0-P0-0.40	32.50	1.51	5.51	5.59
Mean				1.00
COV				0.047

Table 8. Fatigue life comparison of unstrengthened corroded specimens

Specimen	N (×10^4 times)	log$N$	logN_{fit}	log$N$/logN_{fit}
CB-L2-P1-0.55	22.51	5.35	5.31	1.01
CB-L2-P1-0.40	42.21	5.63	5.70	0.99
CB-L2-P1-0.25	200.00	6.30	6.27	1.00
CB-L2-P2-0.55	14.60	5.16	5.15	1.00
CB-L2-P2-0.40	38.81	5.59	5.62	0.99
CB-L2-P2-0.25	200.00	6.30	6.29	1.00
Mean				1.00
COV				0.008

Table 9. Fatigue life comparison of specimen strengthened with polarized C-FRCM plate

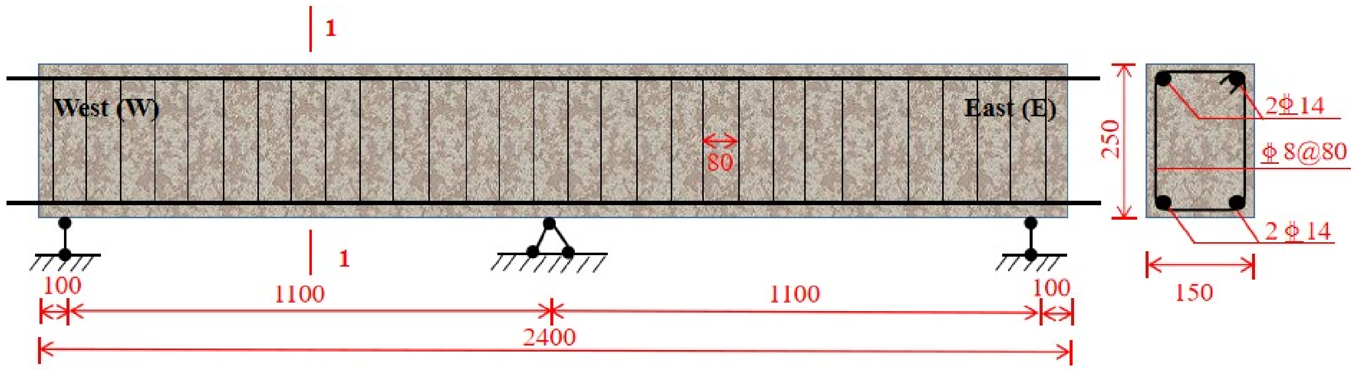

(a) Reinforcement diagram

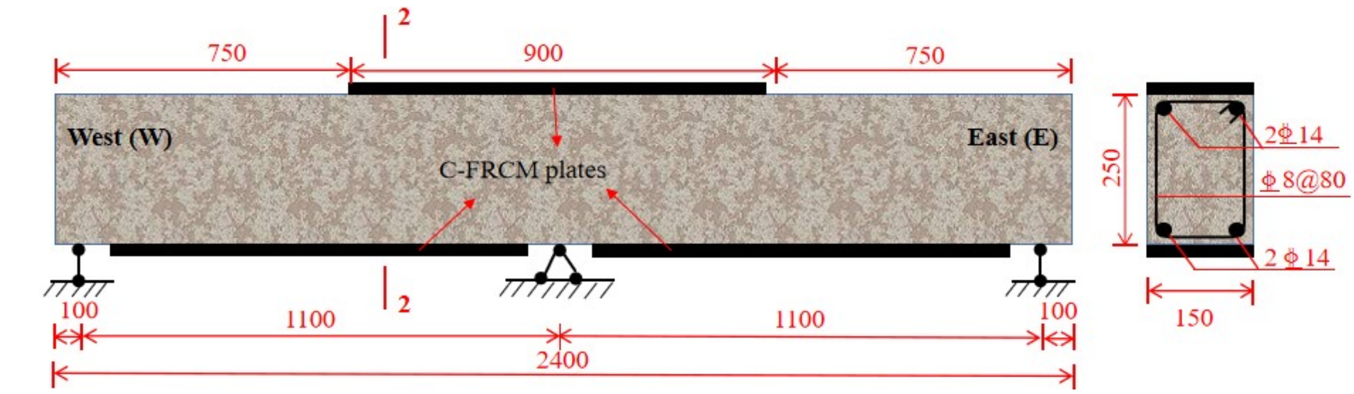

(b) Location of C-FRCM plates

Figure 1. Arrangement of reinforcement and C-FRCM plates for RC continuous beams

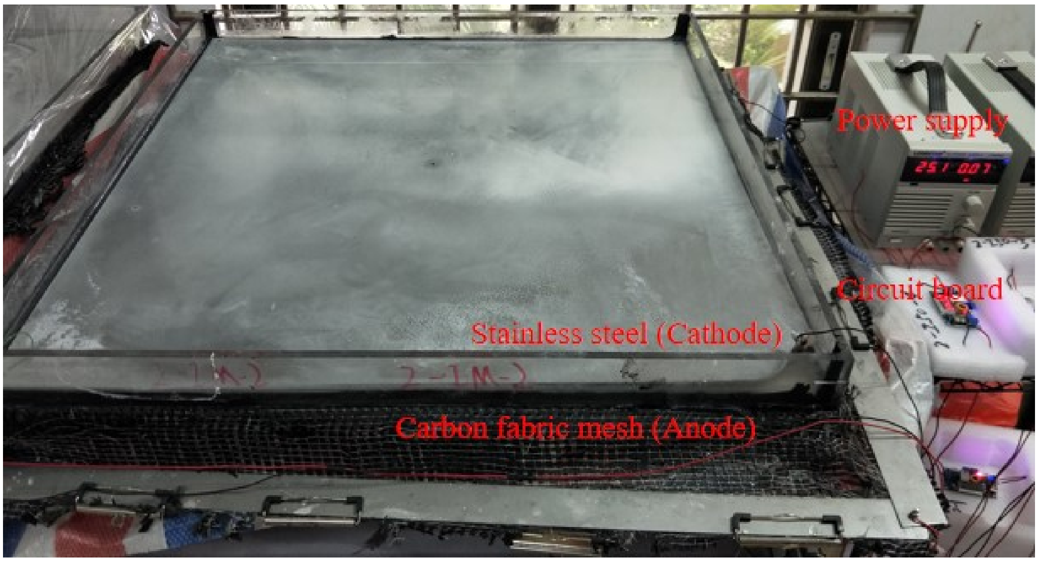

(a) Polarization of C-FRCM plate

(b) Cutting process of C-FRCM plate

(c) Laying of cementitious matrix as adhesive

(d) Removal of air and pores of adhesive

(f) Curing of strengthened beam

Figure 2. Preparation process of RC beams strengthened with C-FRCM plates

(a) Compressive test of concrete cube (b) Flexural test of cementitious matrix

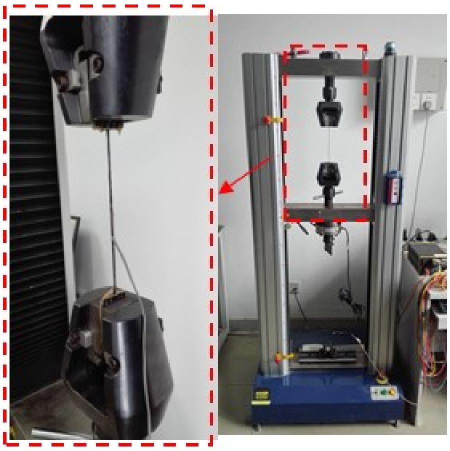

(c) Tensile test of steel bar (d) Tensile test of CF mesh

Figure 3. Material tests

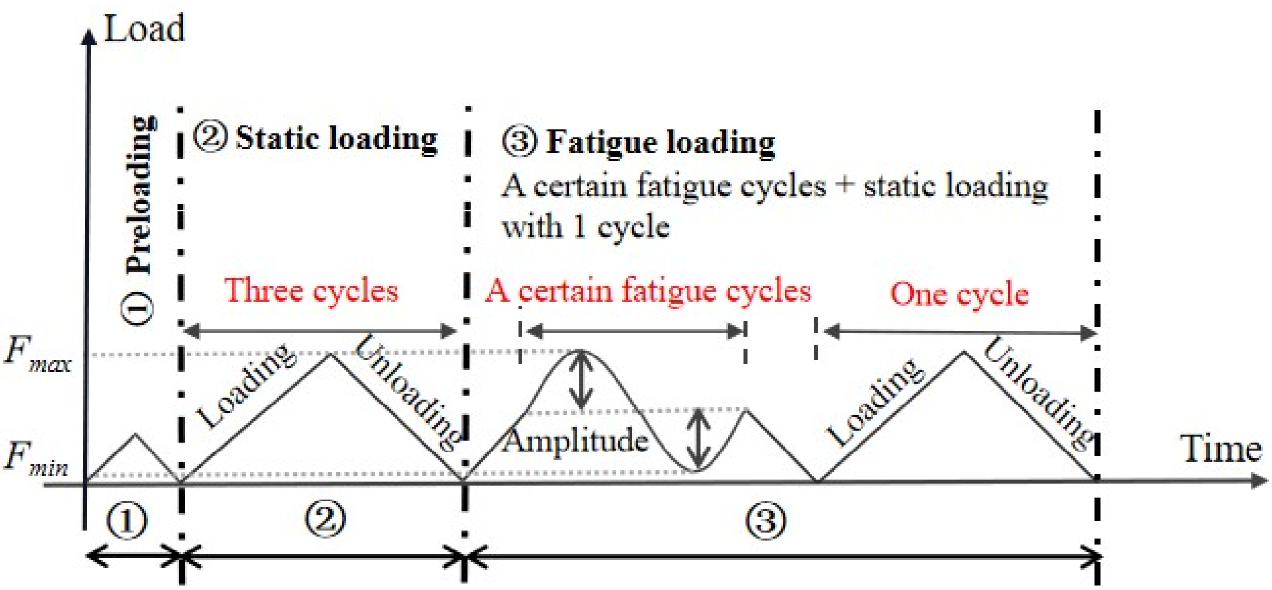

(a) Loading scheme

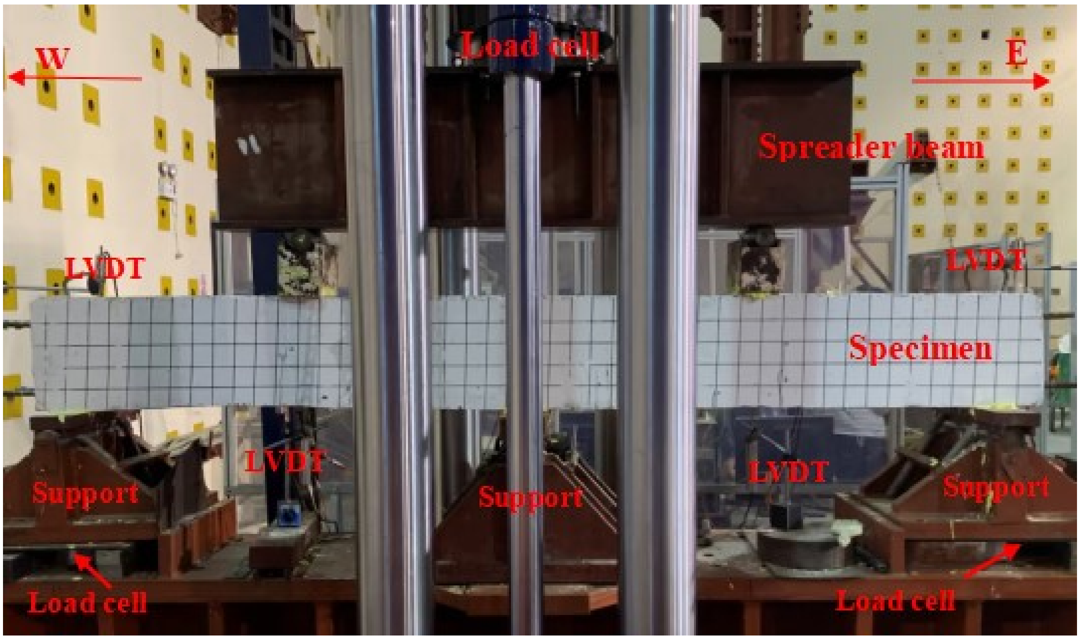

(b) View of test setup

Figure 4. Loading scheme and test setup of fatigue test

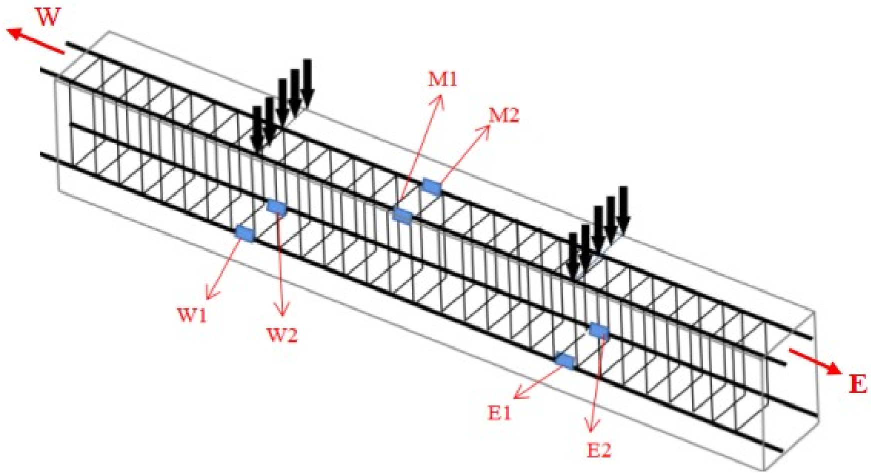

Figure 5. Locations of strain gauges on steel bars

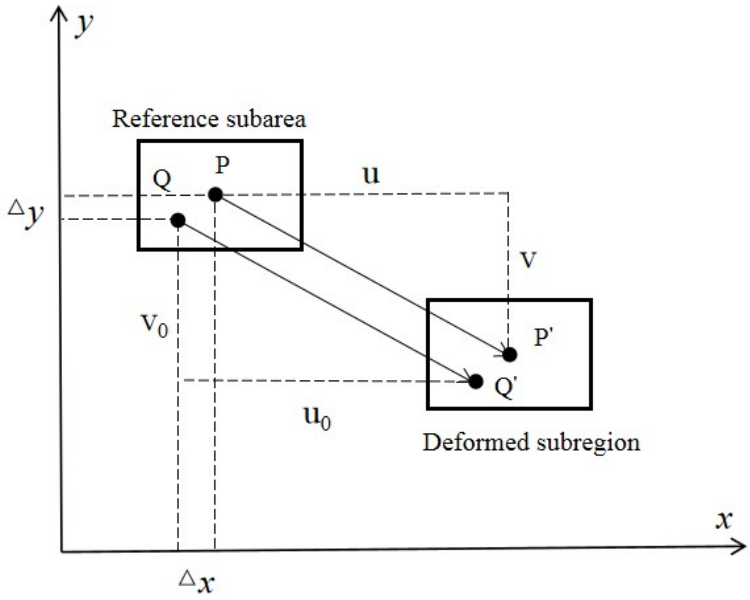

Figure 6. Schematic diagram of displacement analysis in DIC technology

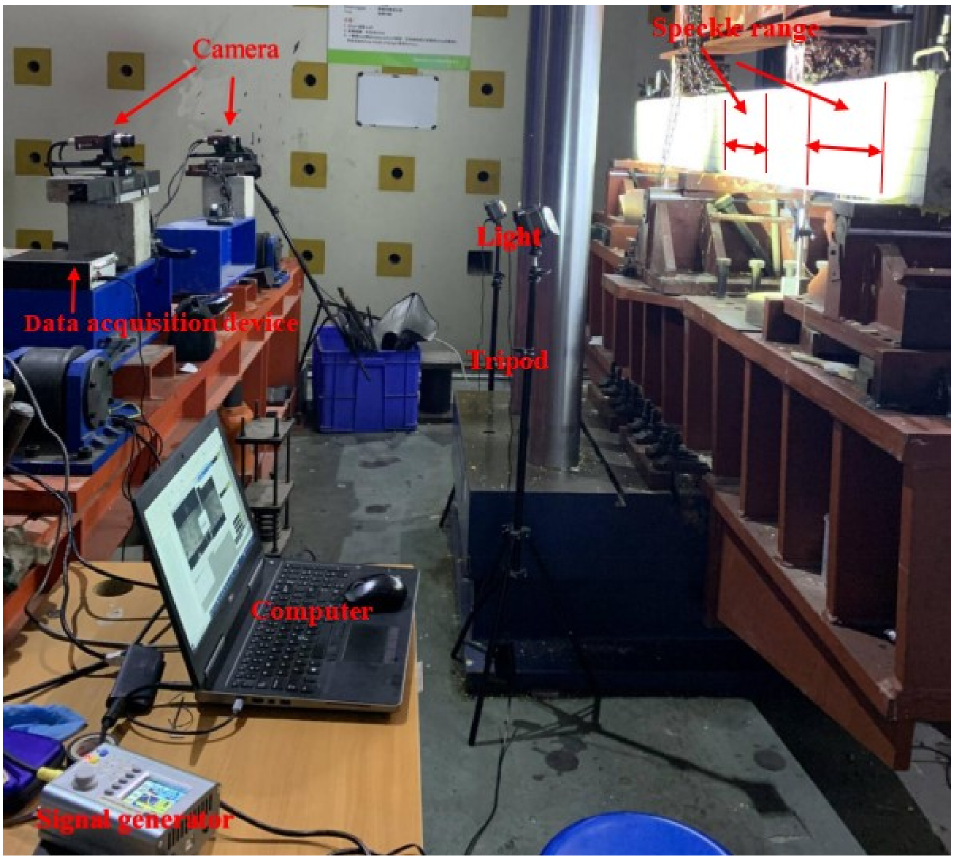

Figure 7. Digital image measuring system

(a) Steel skeleton (b) Comparison before and after rust removal

Figure 8. Steel skeleton and comparison before and after rust removal

(a) Specimen B-L0-P0-0.40

(b) Specimen CB-L0-P0-0.40

(c) Specimen CB-L2-P0-0.40

(d) Specimen CB-L2-P1-0.40

(e) Specimen CB-L2-P2-0.40

Figure 9. Failure modes and cracks development of specimens at a load level of 0.40

(a) Specimen B-L0-P0-0.25

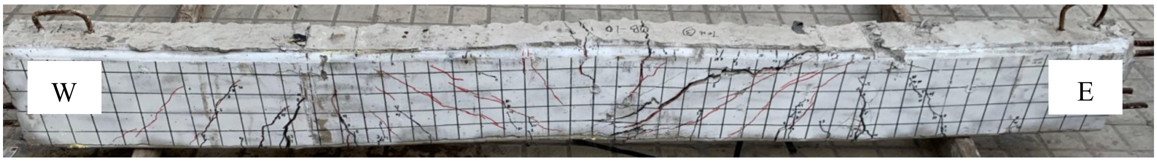

(b) Specimen CB-L0-P0-0.25

(c) Specimen CB-L2-P0-0.25

(d) Specimen CB-L2-P1-0.25

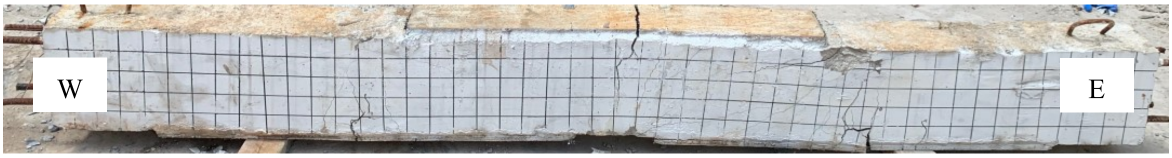

(e) Specimen CB-L2-P2-0.25

Figure 10. Failure modes and cracks development of specimens at a load level of 0.25

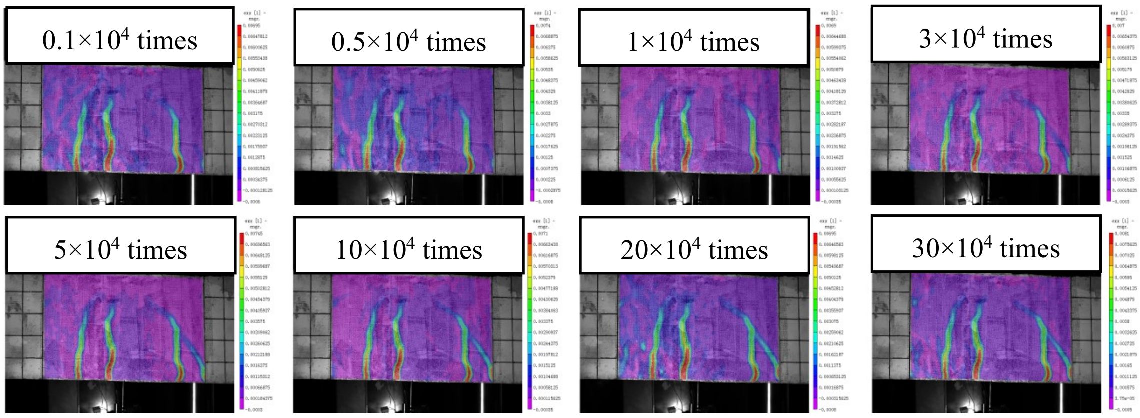

(a) Cracks at mid-span of the west side under certain cyclic loading

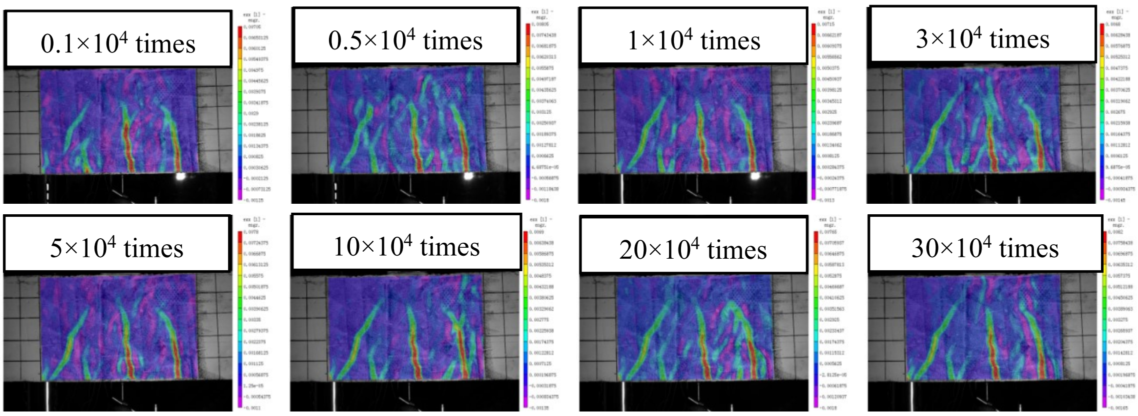

(b) Cracks at mid-span of the east side under certain cyclic loading

Figure 11. Concrete cracks of mid-span under certain cyclic loading

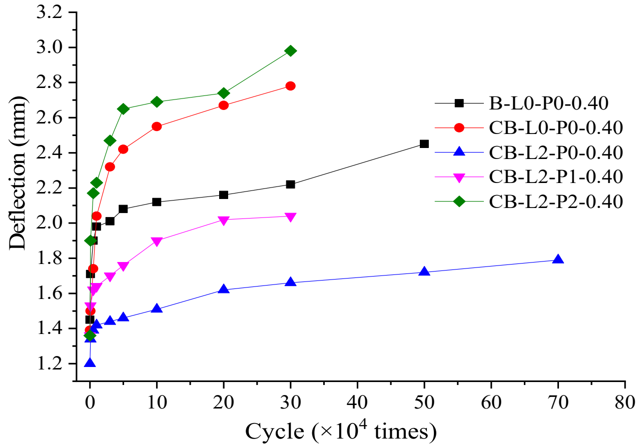

(a) Mid-span of west side at a load level of 0.40

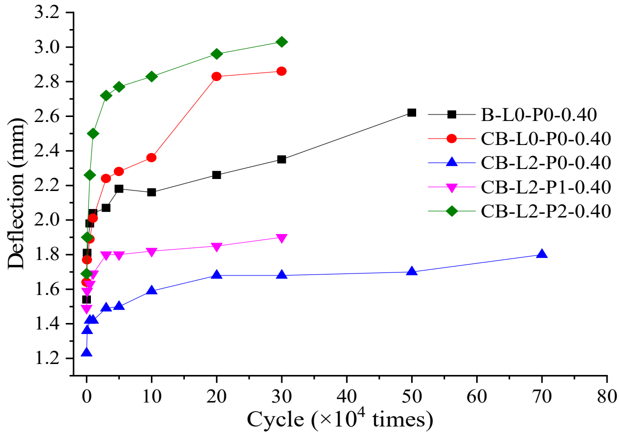

(b) Mid-span of east side at a load level 0.40

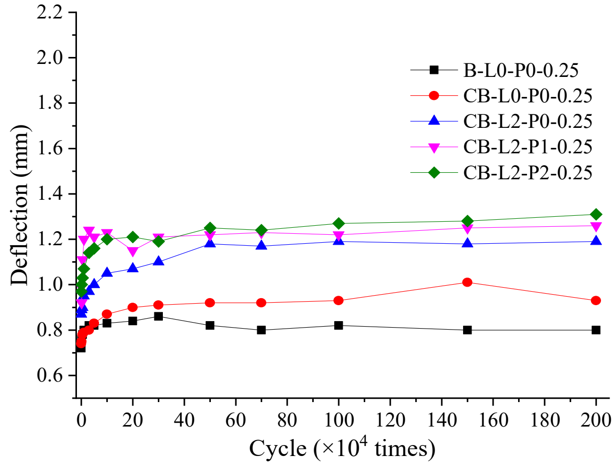

(c) Mid-span of west side at a load level of 0.25

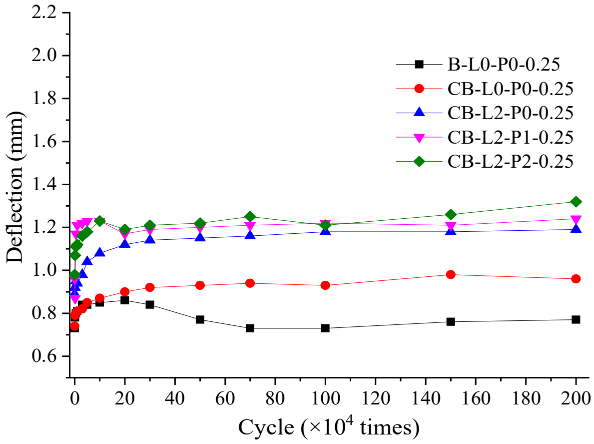

(d) Mid-span of east side at a load level of 0.25

Figure 12. Development of deflection under cyclic loading

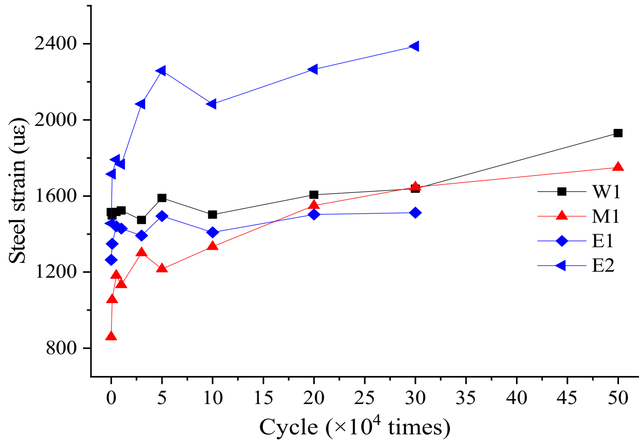

(a) Specimen B-L0-P0-0.40

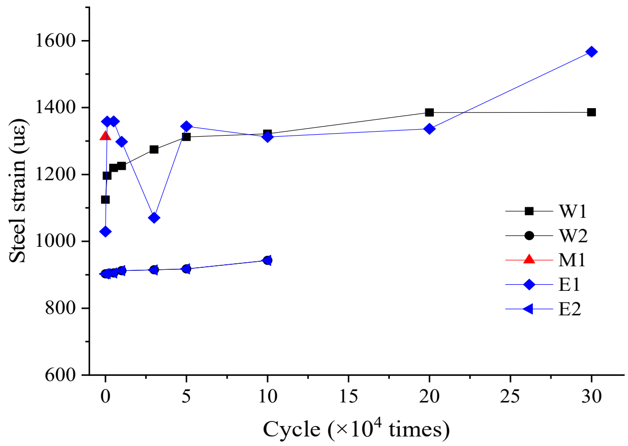

(b) Specimen CB-L0-P0-0.40

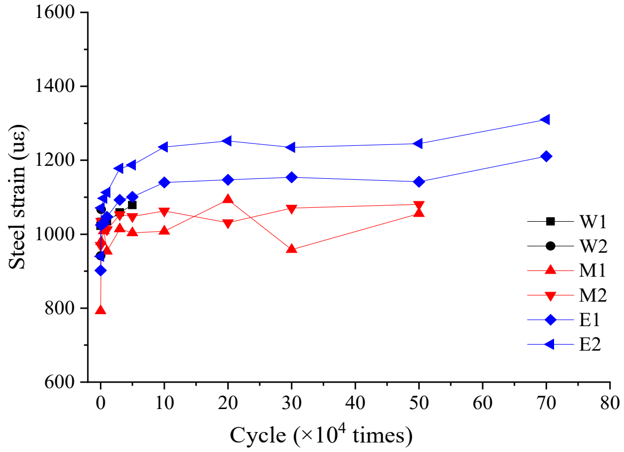

(c) Specimen CB-L2-P0-0.40

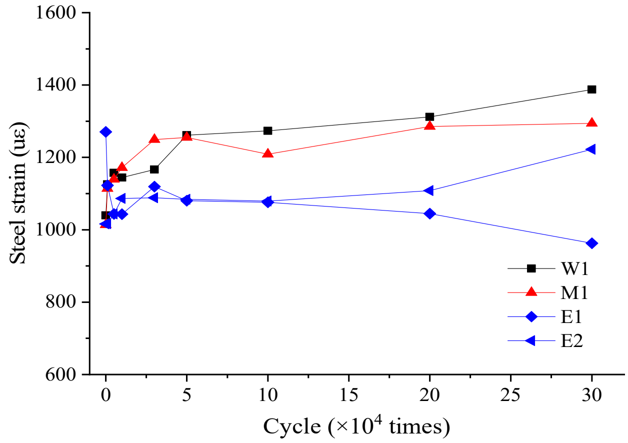

(d) Specimen CB-L2-P1-0.40

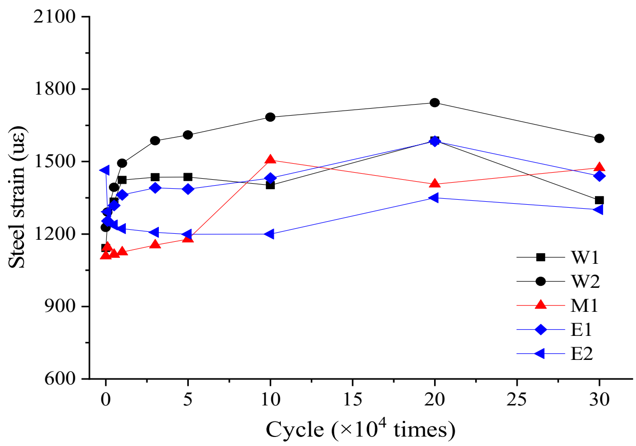

(e) Specimen CB-L2-P2-0.40

Figure 13. Strain development of longitudinal rebars at a load level of 0.40

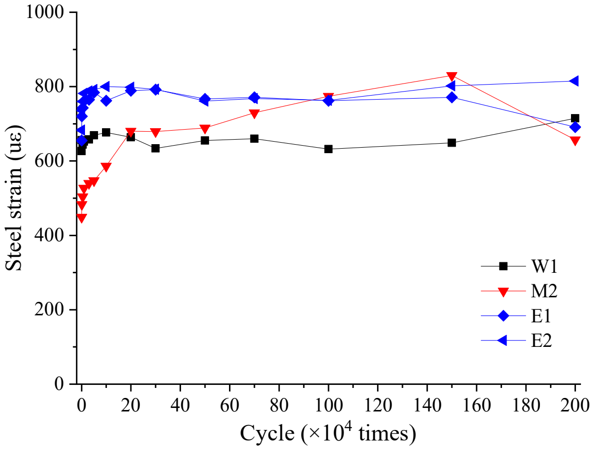

(a) Specimen B-L0-P0-0.25

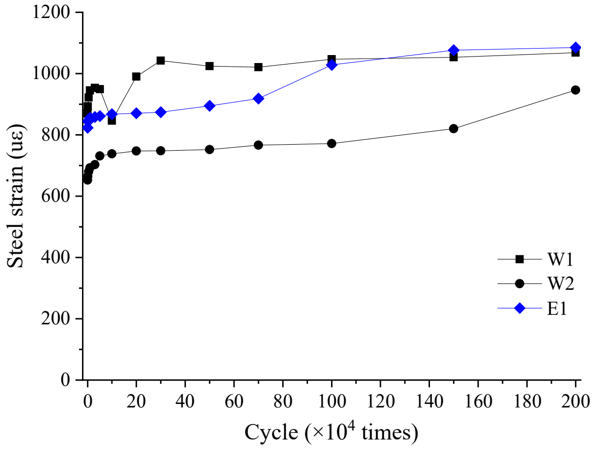

(b) Specimen CB-L0-P0-0.25

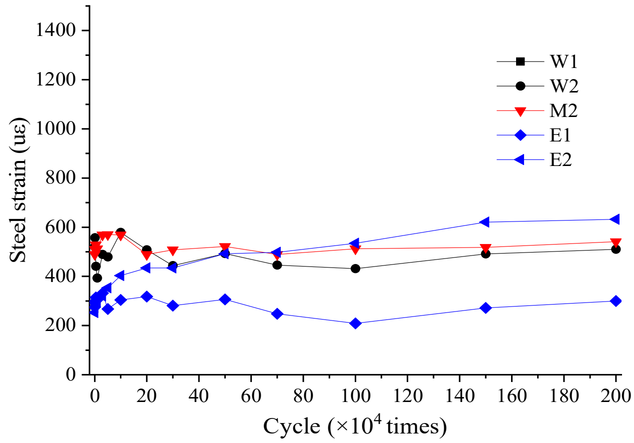

(c) Specimen CB-L2-P0-0.25

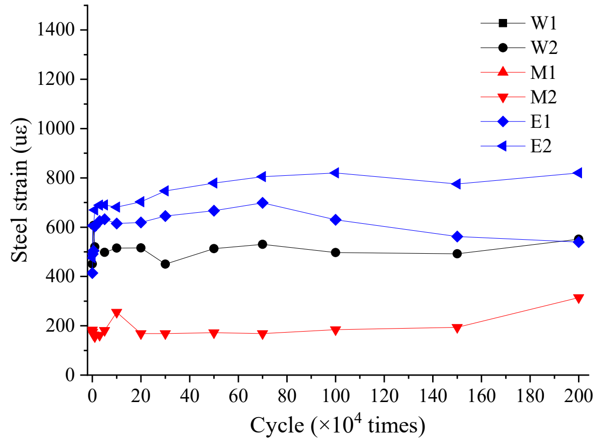

(d) Specimen CB-L2-P1-0.25

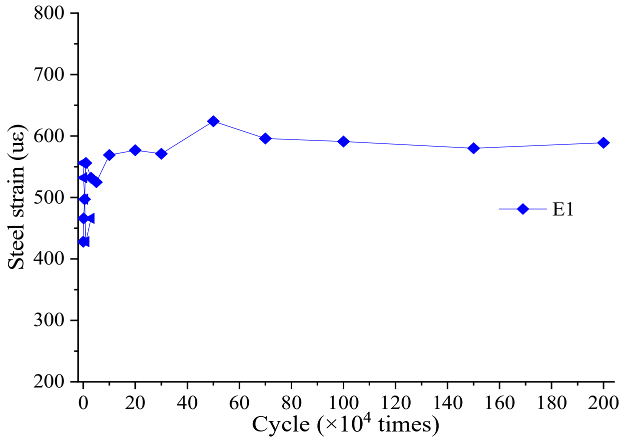

(e) Specimen CB-L2-P2-0.25

Figure 14. Strain development of longitudinal rebars at a load level of 0.25

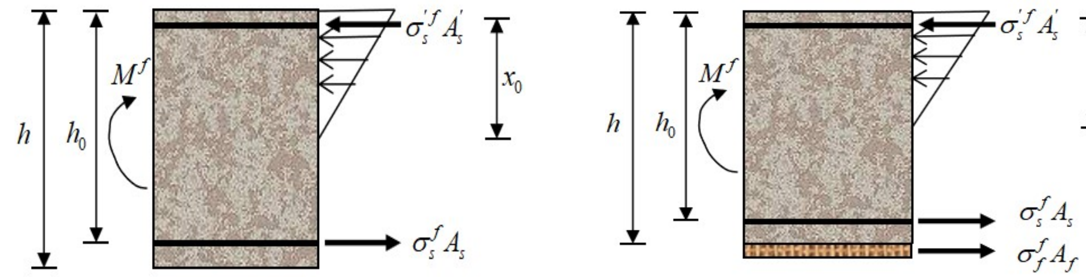

(a) Unstrengthened member (b) Strengthened member

Figure 15. Fatigue stress distribution diagram of normal cross-section of flexural member